Theory of the spin-singlet filling factor $\nu=2$ quantum Hall droplet

Andreas Wensauer,[1,2] Marek Korkusinski,[1] and Pawel Hawrylak[1]

[1]*Institute for Microstructural Sciences, National Research Council Canada, Ottawa, K1A 0R6 Ontario, Canada*
[2]*Institut für Theoretische Physik, Universität Regensburg, D-93040 Regensburg, Germany*

A theory of electronic properties of a spin-singlet quantum Hall droplet at filling factor $\nu=2$ in a parabolic quantum dot is developed. The excitation spectrum and the stability of the droplet due to the transfer of electrons into the second Landau level at low magnetic fields and due to spin flip at the edge at higher magnetic fields are determined using Hartree-Fock, exact diagonalization, and spin-density functional methods. We show that above a critical number of electrons N_c the unpolarized $\nu=2$ quantum Hall droplet ceases to be a ground state in favor of spin-polarized phases. We determine the characteristic pattern in the addition and current-amplitude Coulomb blockade spectra associated with the stable $\nu=2$ droplet. We show that the spin transition of the droplet at a critical number of electrons is accompanied by the reversal of the current-amplitude modulation at the $\nu=2$ line, as observed in recent experiments.

I. INTRODUCTION

In strong magnetic fields, electrons confined in quasi-two-dimensional quantum dots form quantum Hall droplets (QHD).[1] The simplest examples of QHD's are the spin-polarized $\nu=1$ droplet and the spin singlet $\nu=2$ droplet. The $\nu=2$ QHD corresponds to a droplet of electrons occupying the increasing in energy spin-up and spin-down states of the lowest Landau level (LLL).[2] QHDs have been extensively investigated experimentally[2–14] and theoretically.[2,4,8,15–24] Theoretically, the QHD at filling factor $\nu=1$ has attracted most attention.[9,16–20] Experimentally, however, the $\nu=1$ spin-polarized droplet is not easily identified in the Coulomb blockade (CB) addition spectrum.[10] By contrast, the most pronounced feature in the addition spectrum of quantum dots, the $\nu=2$ line, is believed to originate from the formation of the $\nu=2$ QHD.[7] Not surprisingly, recent experiments in quantum dots with controlled electron numbers,[3] and controlled electron numbers combined with spin polarized injection/detection[2] concentrated on the $\nu=2$ QHD. Such a droplet is an example of a chiral Fermi liquid, with both charge and spin excitations, and as such can shed light on the current problem of spin and charge separation in correlated electron systems. Because this droplet is unstable at low magnetic fields against the transfer of electrons to the higher Landau level, it offers new spectroscopic opportunities as well as a more stringent test of various approximations to the quantum dot problem. Despite experimental interest and theoretical opportunities, the detailed physical understanding of the $\nu=2$ QHD in terms of electron numbers, confining energy, magnetic field, and characteristic CB spectrum is rather limited. In this paper we fill this gap and develop a theory of spin singlet QHD at $\nu=2$ in parabolic quantum dots. The parabolic confinement is chosen because it is a general feature of soft confining potentials in gated lateral and vertical devices, as well as in lens-shaped self-assembled quantum dots. The excitation spectrum and the stability of the droplet as a function of the magnetic field, electron number N_e, confining energy ω_0, and Zeeman energy E_z is determined. The spin-singlet $\nu=2$ droplet is found to be unstable due to the transfer of electrons into the second Landau level at low

magnetic fields and due to spin flip at the edge at higher magnetic field. Using Hartree-Fock, spin-density functional, and exact diagonalization methods, we determine the stability conditions of the droplet and the characteristic addition and current-amplitude CB spectrum. We show that above a critical number of electrons N_c, the unpolarized $\nu=2$ quantum Hall droplet ceases to be a ground state in favor of spin-polarized phases. The signature of this transition turns out to be almost invisible in the position of CB peaks, but results in the reversal of the current-amplitude modulation at the $\nu=2$ line with increasing particle number, as observed in recent experiments.[25] We find this reversal to be very sensitive to electronic correlations.

Our paper is organized as follows: In Sec. II we define the single-particle spectrum, the interacting system, and the $\nu=2$ QHD. In Sec. III we analyze the properties of the $\nu=2$ QHD in the lowest Landau level approximation. We calculate the charge and spin excitation spectrum, derive the expressions describing conditions for electron transfer to the second Landau level and for the spin flip at the edge, and calculate the phase diagram. We end with the calculation of the pattern of the addition spectrum characteristic to the $\nu=2$ QHD. In Sec. IV we extend the calculation of the phase diagram to include Landau-level mixing within Hartree-Fock and exact diagonalization methods using one-pair excitations, and spin-density functional theory in the local density approximation (LSDA). Section V is devoted to amplitude modulation patterns expected in spin blockade (SB) spectroscopy. We identify sets of configurations responsible for SB amplitude modulation patterns both in the $\nu=2$ phase and in the region of the phase diagram corresponding to the breakdown of the spin singlet droplet. We show that only inclusion of correlations allows us to obtain reversal of amplitude modulation along the $\nu=2$ line observed in experiment. Sec. VI summarizes our results.

II. THE MODEL

A. Single-particle states and noninteracting electron picture

The energy spectrum $E_{mn\sigma}$ and eigenstates $|m,n,\sigma\rangle$ of an electron localized on a quasi-two-dimensional parabolic
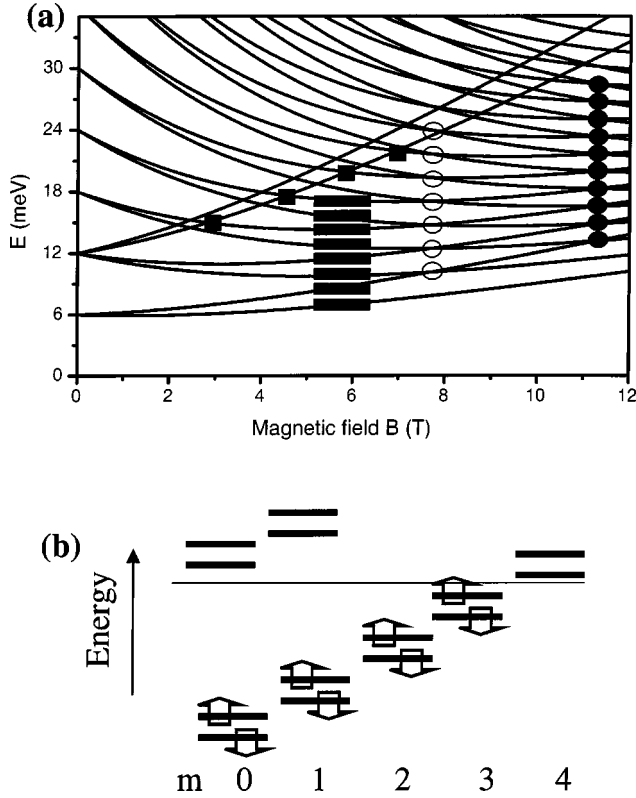
(a)

(b)

FIG. 1. (a) Magnetic-field evolution of single-particle energies for $\omega_0 = 6$ meV and artificially enhanced Zeeman energy $E_Z = 0.15$ meV/T. Circles denote the edge spin flip of a droplet with even (empty) and odd (full) number of electrons. Squares denote the center spin flip. (b) Configuration of noninteracting electrons corresponding to the $\nu = 2$ spin-singlet quantum Hall droplet.
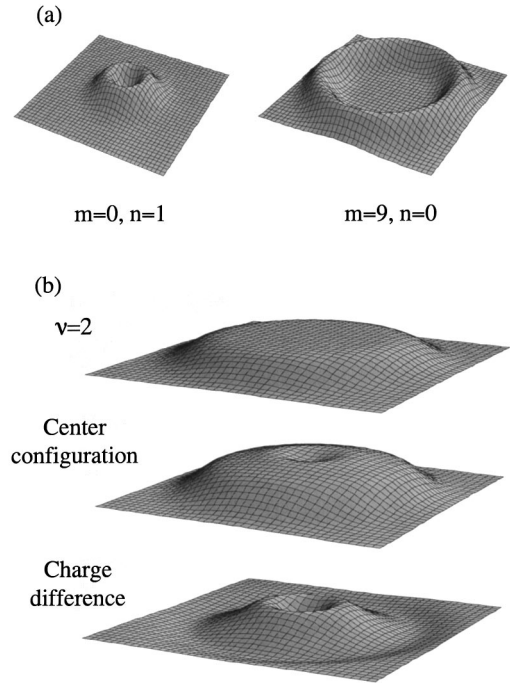

FIG. 2. (a) Probability distribution of single particle orbitals $|0,1\rangle$ (dot center) and $|9,0\rangle$ (dot edge). (b) Charge distribution in the quantum Hall droplet in the center configuration, the $\nu = 2$ phase, and difference in charge distribution of the droplet due to the edge-center transition.

quantum dot are those of two harmonic oscillators in states m,n: $E_{mn\sigma} = \Omega_+ (n + \frac{1}{2}) + \Omega_- (m + \frac{1}{2}) + g\mu \vec{B} \cdot \vec{\sigma}$ and $|m,n;\sigma\rangle = \sqrt{1/m!n!}(a^\dagger)^m (b^\dagger)^n |0,0;\sigma\rangle$, where $a^\dagger$ and $b^\dagger$ are harmonic oscillator operators and σ denotes the electron spin.[15] The magnetic field is directed in antiparalel fashion to the z axis, $\vec{B} = (0,0,-B)$. The two harmonic frequencies are $\Omega_\pm = (\Omega \pm \omega_c)/2$ ($\hbar = 1$ for the rest of this work), $\omega_c = eB/m^*c$ is the cyclotron energy, $l_0 = 1/(m^*\omega_c)^{1/2}$ is the magnetic length, m^* is the effective mass, $\Omega = \sqrt{\omega_c^2 + 4\omega_0^2}$, and the single-particle angular momentum $l = m - n$. Our model calculations will be carried out for GaAs, where the Landé factor $g = -0.44 < 0$, so the Zeeman term $g\mu \vec{B} \cdot \vec{\sigma}$ in negative magnetic fields is negative for spin-down and positive for spin-up electrons. In what follows we denote the Zeeman splitting by $E_z = |g\mu B|$. With increasing magnetic field B the energy Ω_- decreases to zero while Ω_+ increases and approaches cyclotron energy. When the magnetic field increases, the states $|m,n=0\rangle$ evolve into the states of the lowest Landau level while the states $|m,n=1\rangle$ evolve into the states of the second Landau level. The single-particle energy levels $E(m,0,\sigma)$ and $E(0,1,\sigma)$ as a function of the magnetic field B are shown in Fig. 1 (from now on $\sigma_z \equiv \sigma$). For illustration purposes a very high Zeeman energy of $E_Z = 0.15$ meV/T, comparable to the kinetic energy quantization Ω_-, was used. We see that in high magnetic fields

there are low-energy states $|m,0,\pm\rangle$ lower than the lowest-energy orbital $|m=0,n=1\rangle$ of the second Landau level. They form a ladder of states with energies $E_{m,0,\pm} = \Omega_+ (0 + \frac{1}{2}) + \Omega_- (m + \frac{1}{2}) \pm \frac{1}{2}|g|\mu B$. This ladder of states is marked by bars in Fig. 1. When these lowest-energy states are occupied by $N_e = 2N$ electrons, a finite $\nu = 2$ spin-singlet chiral Fermi liquid droplet is formed as shown in Fig. 1(b). In additon to occupied and empty lowest-Landau-level orbitals, there is a parallel ladder of second-Landau-level states $|m,n=1\rangle$ at higher energy. Decreasing the magnetic field lowers the energy of the $|m=0,n=1\rangle$ state with respect to the energy of the highest occupied $|m=N-1,0\rangle$ orbital of the lowest Landau level, and an electron transfer occurs. The $|0,1\rangle$ state to which an electron transfers corresponds to an orbital localized in the center of the dot, while the highest occupied state $|m,0\rangle$ corresponds to an orbital localized at the edge of the droplet. This is illustrated in Fig. 2(a), which shows charge distributions for the states $|0,1\rangle$ and $|9,0\rangle$. In Fig. 2(b) we show the total charge distribution of 14 electrons in the $\nu = 2$ droplet, the distribution after an electron transfers to the center, and the difference of charge distributions between these two configurations. Because the center configuration has one extra electron in the center and a vacancy (hole) at the edge, this charge difference is positive near the center of the dot and negative near the edge of the droplet. Hence the crossing of orbitals leads to the redistribution of electrons from the edge (edge configuration) to the center (center configuration). The crossing, marked by squares in Fig. 1, takes place at different magnetic fields B_1 for different particle numbers. Varying the electron number

allows us to trace this crossing of single-particle levels. This has been pointed out and calculated in a dot with low electron number and strong kinetic energy quantization in Ref. 26. Here we develop such a theory for large numbers of electrons.

With increasing magnetic field the Zeeman splitting becomes larger than the kinetic energy Ω_- and the $\nu=2$ configuration is unstable against a spin flip at the edge.[4] In Fig. 1 this first spin flip is marked by empty circles for even electron numbers and by filled circles for odd electron numbers. We see that spin flips take place at different magnetic fields for even and odd electron numbers. However, for a given parity of the electron number the magnetic field B_2 at which spin flip occurs does not depend on the number of electrons. The center-spin-flip line crosses the edge-spin-flip line at a critical particle number N_c. Hence we might expect that the phase diagram of the $\nu=2$ droplet is finite, i.e., the spin-singlet phase exists only for a finite number of electrons. The rest of the paper will be devoted to developing the understanding of how electron-electron interactions modify this single-particle picture.

3B. The many-particle Hamiltonian

Denoting the creation (annihilation) operators for electrons in states $|m,n;\sigma\rangle$ by $c^\dagger_{mn\sigma}$ ($c_{mn\sigma}$), the Hamiltonian of the interacting system can be written in second quantization as

$$H = \sum_{m,n,\sigma} \varepsilon_{mn\sigma} c^\dagger_{mn\sigma} c_{mn\sigma}$$
$$+ \frac{1}{2} \sum_{m_1 n_1 m_2 n_2 m_3 n_3 m_4 n_4 \sigma\sigma'} \langle m_1 n_1, m_2 n_2 | V | m_3 n_3, m_4 n_4 \rangle$$
$$\times c^\dagger_{m_1 n_1 \sigma} c^\dagger_{m_2 n_2 \sigma'} c_{m_3 n_3 \sigma'} c_{m_4 n_4 \sigma}, \qquad (1)$$

where $\langle m_1 n_1, m_2 n_2 | V | m_3 n_3 m_4 n_4 \rangle$ are the two-body Coulomb matrix elements defined in Ref. 27. The Coulomb matrix elements conserve the angular momentum of the pair during the scattering process: $m_1 - n_1 + m_2 - n_2 = m_3 - n_3 + m_4 - n_4$. They are measured in units of the exchange energy E_0: $E_0 = \mathcal{R}\sqrt{2\pi} a_0 / l_{\text{eff}}$, where $\mathcal{R}$ is the effective Rydberg energy, a_0 is the effective Bohr radius, and $l_{\text{eff}} = l_0 / (1 + 4\omega_0^2/\omega_c^2)^{1/4}$ is the effective magnetic length. The Coulomb energy increases with increasing magnetic field.

III. QUANTUM HALL DROPLET IN THE LOWEST-LANDAU-LEVEL APPROXIMATION

In this section we describe the properties of the $\nu=2$ droplet in the two lowest-Landau-level states neglecting mixing between them. This allows for a number of exact and analytical results that make the physics transparent.

A. Ground state of a QHD with 2N electrons

In the LLL the ground state (GS) of the $\nu=2$ droplet is a product of two spin-polarized droplets:

$$|GS(2N)\rangle = \prod_{m=0}^{N-1} c^\dagger_{m,0\uparrow} \prod_{m=0}^{N-1} c^\dagger_{m,0\downarrow} |0\rangle. \qquad (2)$$

The total number of electrons $N_e = 2N$, and the total angular momentum of the droplet, $R = 2\Sigma_{m=0}^{N-1} m$, are good quantum numbers. In the LLL approximation this state is an exact ground state of the system. It is useful to define electron self-energies $\Sigma(m,n,\sigma)$ at $\nu=2$ for a fixed number of electrons $2N$:

$$\Sigma(m,n,\sigma) = \sum_{m'=0}^{N-1} (2\langle m,n;m',0|V|m',0;m,n\rangle$$
$$- \langle m,n;m',0|V|m,n;m',0\rangle). \qquad (3)$$

This self-energy does not depend on spin, so in what follows the spin index will be dropped. The total energy $E_{\text{GS}}^{2N} = \langle GS(2N)|H|GS(2N)\rangle$ of the $\nu=2$ droplet is now given simply by a sum of energies of quasielectrons:

$$E_{\text{GS}}^{2N} = \sum_{m=0}^{N-1} 2\left[\Omega_-\left(m+\frac{1}{2}\right) + \frac{1}{2}\Omega_+\right] + \Sigma(m,0). \qquad (4)$$

The electrons are replaced by quasiparticles (electrons dressed with interactions).

B. Excitation spectrum and spectral functions of the QHD with 2N electrons

Let us now analyze the charge and spin excitation spectrum of the $\nu=2$ droplet in the LLL. The one-electron charge and spin excited states $|dm,m,\pm\rangle$ can be labeled by the increase of angular momentum dm with respect to the $\nu=2$ state. We construct them by removing one electron from one of the occupied states $|m,\sigma\rangle$ and putting it onto one of the unoccupied states $|m+dm,\sigma\rangle$:

$$|dm,m,\pm\rangle = \frac{1}{\sqrt{2}}[c^\dagger_{m+dm,0,\downarrow} c_{m,0,\downarrow}$$
$$\pm c^\dagger_{m+dm,0,\uparrow} c_{m,0,\uparrow}]|GS(2N)\rangle, \qquad (5)$$

where $+$ refers to the spin singlet (charge excitation) and $-$ to the spin triplet (spin excitation). To understand the difference between the two excitations we discuss the lowest angular momentum excited states $dm=+1$. The spin-singlet excitation can be obtained by acting on the $\nu=2$ droplet with the center-of-mass operator $Q^\dagger = \Sigma_{m,\sigma}(m+1)^{1/2} c^\dagger_{m+1,0,\sigma} c_{m,0,\sigma}$. The energy of this excitation, measured from the energy of the $\nu=2$ state, equals exactly the kinetic energy Ω_-, or the energy needed to increase the angular momentum of one electron by one unit. This is exactly what one finds for the $\nu=1$ state. The spin-triplet excitation, on the other hand, has the energy of the charge excitation minus twice the exchange energy across the Fermi level $N-1$, i.e., $\Omega_- - 2\langle N-1;N|V|N-1;N\rangle$. Hence, the spin-triplet excitations have an energy lower than that of the charge excitations.

The excitation spectrum can be probed by adding one electron to the droplet. The probability of adding an electron
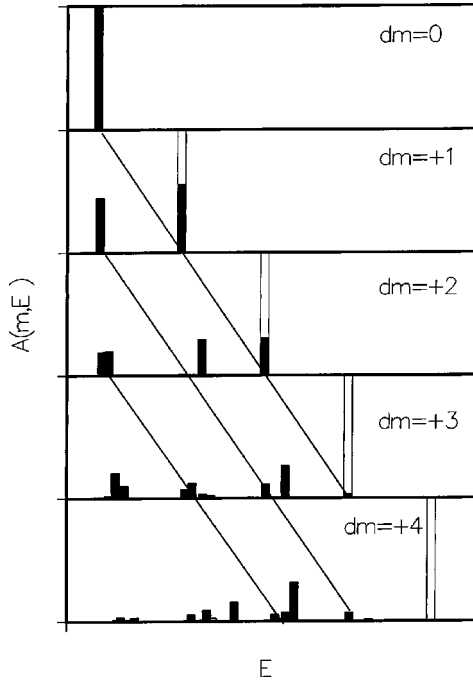
FIG. 3. Spectral function of the $\nu=2$ droplet with $N=8$ in the lowest Landau level approximation.

to the orbital $|m,0\rangle$ with energy E is given by the spectral function[24] $A(m,E)=\Sigma_f|_f\langle 2N+1|c_{m,\downarrow}^\dagger|GS(2N)\rangle|^2\delta(E_f(2N+1)-E_0(2N)-E)$. The electron probes all excited final states of the $2N+1$ droplet, a reflection of the excitation spectrum of the $2N$ droplet. In Fig. 3 we show an example of the calculated spectral function of a $2N=8$ electron droplet at $\nu=2$ obtained by exact diagonalization techniques[4,24] for $\omega_c/\omega_0=0.2$. The spectral function of the noninteracting system describes an addition of an electron to empty states with energy spacing Ω_- and probablity of 1. In a Fermi liquid this noninteracting picture would be only slightly modified by interactions. However, in the quantum dot the quasiparticle picture breaks down already at the first excited state, and for the energy $\sim 3\Omega_-$ the spectral function is already almost zero. Moreover, we see that even though there are many more states than in the noninteracting picture, these states form bunches which leads to a discrete density of states. The bunching and the separation of bunches are controlled by Coulomb interactions rather than by the single-particle energy levels.

C. Spin-flip excitation spectrum of QHD with 2N electrons

Let us now turn to a detailed analysis of the spin-flip excitations of the $\nu=2$ droplet. We start with the center configuration. It involves an electron transfer from the highest occupied orbital of the lowest Landau level to the lowest-energy state of the second Landau level accompanied by a spin flip: $|C(2N)\rangle=c_{0,1,\downarrow}^\dagger c_{N-1,0,\uparrow}|GS(2N)\rangle$. This state corresponds to two electrons with parallel spin (triplet state), one in the center of the droplet and one at the edge. There is only one state with this angular momentum and spin in the subspace of one-pair excitations on two Landau levels, so

this is an exact eigenstate of the Hamiltonian. The two electrons involved cannot be distinguished from the rest of electrons. To account for all electrons it is better to think of a created electron as a quasielectron and a removed electron as a quasihole. The energy of the electron-hole pair is given by a difference in the energy of a quasielectron in the center orbital and a quasihole at the edge of the droplet plus their attraction:

$$E(C)^{2N}=E_{GS}^{2N}+\left(\Omega_+ +\Sigma(0,1)-\frac{1}{2}E_z\right)$$
$$-\left((N-1)\Omega_-+\Sigma(N-1,0)+\frac{1}{2}E_z\right)$$
$$-\langle N-1,0;0,1|V|0,1;N-1,0\rangle. \qquad (6)$$

The energy of the quasielectron and quasihole pair depends on the total number of electrons in the $\nu=2$ droplet. This interpretation of the triplet state as a collective state differs from the two-electron model of Tarucha *et al.*[3] When the magnetic field B is lowered beyond a critical value B_1, the energy of the center configuration becomes lower than the energy of the $\nu=2$ configuration, the $\nu=2$ spin-singlet droplet becomes unstable, and a spin-triplet center configuration becomes the ground state.

We now turn to the breakdown of stability of the droplet due to spin flip at the edge. The spin-flip wave functions can be generated from the droplet at filling factor $\nu=2$ by removing a spin up electron at $|N-1,0\rangle$ and creating a spin-down electron at the first available state at the edge $|N,0\rangle$ (a spin exciton): $|E(2N)\rangle=c_{N,0,\downarrow}^\dagger c_{N-1,0,\uparrow}|GS(2N)\rangle$. The process described here is equivalent to creating a hole (a missing spin-up electron) below the Fermi level, and a spin-down electron at the edge. Similarly to Eq. (6), we can easily calculate the energy of this configuration:

$$E(E)^{2N}=E_{GS}^{2N}+\Omega_- -E_z+\Sigma(N,0)-\Sigma(N-1,0)$$
$$-\langle N-1,0;N,0|V|N,0;N-1,0\rangle. \qquad (7)$$

As compared to the energy of the $\nu=2$ droplet, the energy of the edge spin-flip exciton is increased by the kinetic energy Ω_-, and lowered by the Zeeman energy. The quasielectron and the quasihole are dressed by their self-energies, and they attract each other. As the magnetic field is increased, the energy of the edge-spin-flip configuration becomes lower than the energy of the $\nu=2$ spin-singlet droplet, and the triplet edge configuration becomes the ground state. The magnetic field at which this takes place will be referred to as B_2. The calculated difference of self-energies across the Fermi level is much smaller than the vertex correction, which controls the value of the magnetic field where the spin flip occurs. The vertex correction in turn depends on N, hence B_2 depends on the number of electrons.

D. Phase diagram of QHD with 2N electrons

We can now use Eqs. (6) and (7) to determine the critical magnetic fields B_1 and B_2 as a function of the number of electrons $N_e=2N$ for different confinement energies ω_0 (in-
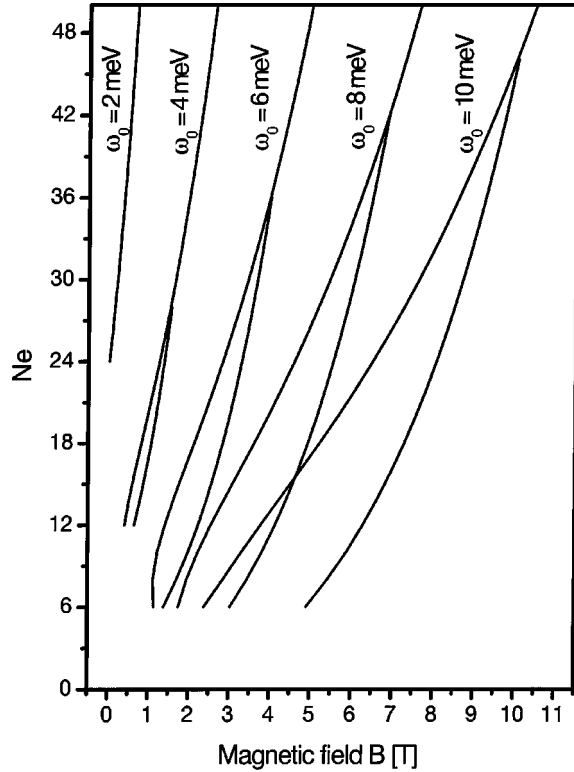
FIG. 4. Phase diagram of the even-electron droplet as a function of electron number and the magnetic field in the lowest-Landau-level approximation and for different confinement energies.

dependent of N) and Zeeman energy $E_z = 0.02$ meV/T appropriate for GaAs. For the GaAs Zeeman energy and, e.g., $\omega_0 = 6$ meV, the Zeeman splitting of single-particle levels in Fig. 1 would now be barely visible, and no spin flips would occur in the experimentally accessible range of magnetic fields. Then, the model of noninteracting electrons would not allow for edge spin flips;[4] however, the center-spin-flip transition would still be possible. The inclusion of interactions modifies this picture. The calculated phase diagrams are shown in Fig. 4. We find that the stability of phases is strongly affected by ω_0 to the extent that the $\nu = 2$ phase does not seem to be stable for $\omega_0 < 4$ meV. For larger confinement energies the phase diagram qualitatively resembles the noninteracting phase diagram of Fig. 1. Quantitatively, the main difference between these two approaches is visible in the behavior of the $\nu = 2$ edge-spin-flip phase boundary, independent on the number of electrons in the noninteracting

picture, but strongly affected by the size of the droplet of interacting electrons. Also, in the single-particle picture the center-spin-flip $\nu = 2$ phase boundary has a parabolic shape (traces the kinetic energy of the $|0,1,\downarrow\rangle$ orbital), which is not preserved in Fig. 4. The key observation common to both approaches is that for any $\omega_0 > 4$ meV the $\nu = 2$ phase is stable only up to a critical number of electrons N_c. This critical number of electrons increases with increasing ω_0. Thus, a large droplet is expected to consist of a bulk $\nu = 2$ core and a spin-polarized edge.

E. Quasielectron in QHD with $2N+1$ electrons

In transport experiments one does not measure directly the energies of configurations discussed above. The measured quantity is the chemical potential, i.e., the difference between the ground state energies of the $(2N+1)$- and $2N$-electron droplet.[15] Therefore now we must discuss the system of $2N+1$ electrons, where we consider the extra electron as a quasielectron added to the $N_e = 2N$ electron droplet.

The ground state configuration consists of the $\nu = 2$ droplet and an extra electron on the $|N,0\rangle$ orbital. The energy of this state is the energy of the $\nu = 2$ droplet plus the energy of the quasielectron:

$$E_{\mathrm{GS}}^{2N+1} = E_{\mathrm{GS}}^{2N} + \left(N + \frac{1}{2}\right)\Omega_- + \frac{1}{2}\Omega_+ - \frac{1}{2}E_z + \Sigma(N,0),$$
(8)

which includes the self-energy evaluated for the $2N$-electron droplet.

The center configuration is obtained by transferring the quasielectron to the center orbital. The energy of this configuration is given by

$$E(C)^{2N+1} = E_{\mathrm{GS}}^{2N} + \frac{1}{2}\Omega_- + \left(1 + \frac{1}{2}\right)\Omega_+ - \frac{1}{2}E_z + \Sigma(0,1).$$
(9)

The first spin-flip state can be generated from the droplet at filling factor $\nu = 2$ and a quasielectron at the edge by removing a spin-up electron at $|N-1,0\rangle$ and creating a spin-down electron at the first available state at the edge, i.e., $|N+1,0\rangle$. This is the $\nu = 2$ configuration with one hole and two additional spin-down electrons at the edge, a spin-flip trion, whose energy is given by

$$E(E)^{2N+1} = E_{\mathrm{GS}}^{2N} + \left[\left(N + \frac{1}{2}\right)\Omega_- + \frac{1}{2}\Omega_+ - \frac{1}{2}E_z + \Sigma(N,0)\right] + \left[\left(N + 1 + \frac{1}{2}\right)\Omega_- + \frac{1}{2}\Omega_+ - \frac{1}{2}E_z + \Sigma(N+1,0)\right]$$

$$- \left[\left(N - 1 + \frac{1}{2}\right)\Omega_- + \frac{1}{2}\Omega_+ + \frac{1}{2}E_z + \Sigma(N-1,0)\right] - \langle N-1,0;N,0|V|N,0;N-1,0\rangle$$

$$- \langle N-1,0;N+1,0|V|N+1,0;N-1,0\rangle + \langle N+1,0;N,0|V|N,0;N+1,0\rangle - \langle N+1,0;N,0|V|N+1,0;N,0\rangle.$$
(10)

The energy of the first spin-flip configuration for odd electron numbers is a sum of the energies of a quasielectron at $m=N$, a quasielectron at $m=N+1$, a quasihole at $m=N-1$, the attractive interaction of electrons with a quasihole, and the direct and exchange interaction among the two electrons of the trion. In analogy to the $2N$-electron case, we expect to observe ranges of magnetic field in which each of these three configurations becomes the ground state of the QHD.

F. Addition spectrum

We can now calculate the addition spectrum (chemical potential) of the $2N$-electron droplet, defined as $\mu(2N) = E(2N+1) - E(2N)$. The chemical potential as a function of the magnetic field exhibits features corresponding to changes in the ground state energies of the $2N$ and of $2N+1$ droplet. Let us start with the $\nu=2$ $2N$ droplet and add an extra quasielectron at the edge. The addition energy to do so, or the chemical potential in this magnetic field range,

$$\mu_3(2N)=E_{\text{GS}}^{2N+1}-E_{\text{GS}}^{2N}=N\Omega_- + \frac{1}{2}\Omega - \frac{1}{2}E_z + \Sigma(N,0),$$
(11)

is a sum of the kinetic energy and self-energy at the edge of the droplet. The kinetic energy contribution *increases* with decreasing magnetic field. At a critical value B_1^* of the magnetic field the quasielectron transfers from the edge to the center of the dot (transition in the $2N+1$ droplet), while the $2N$-electron droplet remains stable. In this new configuration the addition energy

$$\mu_2(2N)=E(C)^{2N+1}-E_{\text{GS}}^{2N}=\Omega_+ + \frac{1}{2}\Omega - \frac{1}{2}E_z + \Sigma(0,1)$$
(12)

is a sum of the kinetic and the self-energy $\Sigma(0,1)$ of the quasielectron in the center of the droplet. The energy to add a quasi-electron to the center is proportional to Ω_+ and *decreases* with decreasing magnetic field. Therefore the chemical potential has an upward cusp at $B=B_1^*$.

When the magnetic field is lowered below B_1, the $2N$-electron droplet becomes unstable and a spin-triplet magnetoexciton center configuration is formed. The magnetoexciton consists of an electron in the center and a hole at the edge. The electron in the center cancels out in the additon spectrum and the chemical potential now measures the energy of a "dressed" quasihole at the edge of the $2N$ droplet, the "dressing" coming from final state correction in the form of electron-hole attraction:

$$\mu_1(2N)=E(C)^{2N+1}-E(C)^{2N}=\frac{1}{2}\Omega+(N-1)\Omega_- + \frac{1}{2}E_z$$
$$+\Sigma(N-1,0)+\langle N-1,0;0,1|V|0,1;N-1,0\rangle.$$
(13)

The kinetic energy of this hole *increases* with decreasing magnetic field. This tendency is somewhat compensated by the interactions. Hence, at $B=B_1$ the addition spectrum exhibits a downward cusp.

Consider now the addition of one electron to an odd, $(2N-1)$-electron droplet. In high magnetic fields the initial state consists of the $\nu=2$ droplet and a hole on the missing spin up state at the edge. The final state is the $2N$-electron $\nu=2$ droplet. Thus the extra electron is added to the edge. Its energy is proportional to Ω_- (renormalized by interactions which depend weakly on the magnetic field); therefore the chemical potential *increases* with the decreasing magnetic field. As we lower the magnetic field, the final state of $2N$ electrons undergoes the first transition at $B=B_1$: the center configuration becomes stable. The extra electron occupies the center orbital, the chemical potential in this regime *decreases* with decreasing magnetic field, and the addition spectrum will exhibit a cusp pointing up. Note that this cusp will be seen at exactly the same magnetic field as the downward cusp described previously for the addition of an extra electron to the even, $2N$-electron QHD. Finally, both initial and final configurations contain a center electron. Then, the addition of a spin-down electron takes place at the edge, and the chemical potential exhibits a downward cusp and begins to *increase* with decreasing magnetic field.

In Fig. 5 we show the calculated chemical potentials for a droplet with $N=16-21$ electrons, with charging energy subtracted. Each addition spectrum contains a segment with energy increasing with increasing magnetic field. We see that the spacing between consecutive pairs of addition curves oscillates between large and small. For addition spectrum of a quasielectron to a $2N$-electron droplet, the spacing corresponds to a difference between the energy to add a quasielectron with spin down and the energy to add a quasihole with spin down (electron with spin up below the Fermi level). In the interacting system, the electron and a quasihole are dressed by interactions. The energy difference, Δ_L, is the difference in the chemical potential $\Delta_L = \mu_3(2N) - \mu_1(2N)$:

$$\Delta_L = \Omega_- - E_z + \Sigma(N,0) - \Sigma(N-1,0)$$
$$-\langle N-1,0;0,1|V|0,1;N-1,0\rangle.$$
(14)

Because this energy corresponds to a quasielectron above the Fermi level and a quasihole below, it includes the kinetic and self-energy difference across the Fermi level, plus excitonic correction. This is the final state interaction correction in the spectroscopy involving transfer of electron from the edge into the center of the dot by decreasing magnetic field. The two spins are opposite and we also have to subtract the Zeeman energy. In a noninteracting system the spacing is proportional to $\Omega_- - E_z$.

Similar arguments can be used for the derivation of the other energy difference, Δ_S, in the addition spectrum of the odd electron number, $2N-1$ droplet:

$$\Delta_S = E_z + \langle N-1,0;N-1,0|V|N-1,0;N-1,0\rangle$$
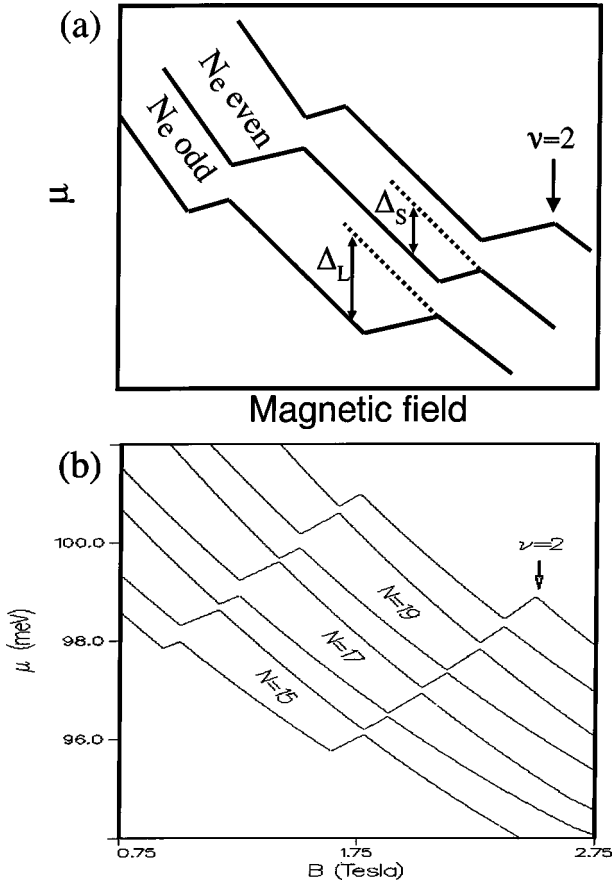$$-\langle N-1,0;0,1|V|0,1;N-1,0\rangle.$$
(15)

FIG. 5. (a) Schematic view of the chemical potentials for odd and even number of electrons indicating the energy differences Δ_L and Δ_S discussed in the text. (b) Addition spectrum of a quantum dot in a spin blockade experiment (Ref. 28).

The spacing for the odd electron droplet is proportional only to the Zeeman energy and excitonic corrections. If interactions are weak, this spacing should be much smaller than the spacing for even electron droplets. Therefore calculations predict a characteristic pattern in the addition spectrum of the $\nu=2$ droplet related to the even or odd number of electrons in the droplet. This pattern, measured experimentally,[28] is expected to be valid only for electron numbers $N_e < N_c$.

IV. LANDAU LEVEL MIXING AND EXCHANGE AND CORRELATION EFFECTS IN QHD

In the preceding section we were able to derive a number of rigorous results by restricting Hilbert space to states derived from the two lowest Landau levels without their mixing. We now turn to include Landau level mixing and correlations.

A. Hartree-Fock calculations in two LLL's

We start with the Hartree-Fock (HF) calculations, whose simplest example involves only two Landau levels. We write the $\nu=2$ HF wave function as a product of variational wave functions in each spin channel σ and angular momentum channel m:

$$|GS(2N)\rangle = \prod_{\sigma} \prod_{m=0}^{N-1} (a_{m,0,\sigma}^* c_{m,0,\sigma}^\dagger + a_{m,1,\sigma}^* c_{m+1,1,\sigma}^\dagger)|0\rangle. \quad (16)$$

The N coefficients $a_{m,0,\sigma}^*$ and $a_{m,1,\sigma}^*$, $m=0,1,\ldots,N-1$ are determined by either minimizing the total energy subject to normalization of the wave function or by solving the eigenvalue problem of the HF Hamiltonian. The HF Hamiltonian is defined by noting that the HF wave function allows us to define expectation values $\rho_{i,j} = \langle c_i^\dagger c_j \rangle$ of the density matrix in terms of the coefficients $a_{m,0,\sigma}^*$, $a_{m,1,\sigma}^*$. For example, $\langle c_{m,0,\sigma}^\dagger c_{m,0,\sigma} \rangle = a_{m,0,\sigma}^* a_{m,0,\sigma}$, $\langle c_{m+1,1,\sigma}^\dagger c_{m+1,1,\sigma} \rangle = a_{m,1,\sigma}^* a_{m,1,\sigma}$, are simply occupations of the HF level 0 and the HF level 1 in the angular momentum channel m, while $\langle c_{m+1,1,\sigma}^\dagger c_{m,0,\sigma} \rangle = a_{m+1,1,\sigma}^* a_{m,0,\sigma} = p_{m,\sigma}^*$ are off-diagonal elements (polarizations) of the density matrix. Replacing the two-body term in Eq. (1) by a one-body and mean-field term the HF Hamiltonian reads:

$$H = \sum_{m,n\sigma} \varepsilon_{m,n\sigma} c_{m,n\sigma}^\dagger c_{m,n\sigma}$$

$$+ \sum_{m_1 n_1 m_2 n_2 m_3 n_3 m_4 n_4 \sigma\sigma'} \langle m_1 n_1, m_2 n_2 | V | m_3 n_3, m_4 n_4 \rangle$$

$$\times (c_{m_1 n_1 \sigma}^\dagger \langle c_{m_2 n_2 \sigma'}^\dagger c_{m_3 n_3 \sigma'} \rangle c_{m_4 n_4 \sigma}$$

$$- c_{m_1 n_1 \sigma}^\dagger \langle c_{m_2 n_2 \sigma'}^\dagger c_{m_4 n_4 \sigma} \rangle c_{m_3 n_3 \sigma'}). \quad (17)$$

The HF Hamiltonian can be further simplified by separating individual angular momentum and spin channels. Neglecting the spin dependence, the effective Hamiltonian in a channel $l = m - n$ is simply a 2×2 matrix:

$$H_{HF} = \begin{bmatrix} \varepsilon_0(l) + V_{0,0}(l) & V_{0,1}(l) \\ V_{0,1}(l) & \varepsilon_1(l) + V_{1,1} \end{bmatrix}, \quad (18)$$

where $V_{i,j}(l)$ are self-consistent HF fields. For example, $V_{0,0}(l=m)$ reads

$$V_{0,0}(l=m) = \sum_k \langle m,0;k,0 | V_{dx} | k,0;m,0 \rangle a_{m,0}^* a_{m,0}$$

$$+ \langle m,0;k+1,1 | V_{dx} | k+1,1;m,0 \rangle a_{m,1}^* a_{m,1}$$

$$+ \langle m,0;k+1,1 | V_{dx} | k,0;m,0 \rangle a_{m,1}^* a_{m,0}$$

$$+ \langle m,0;k,0 | V_{dx} | k+1,1;m,0 \rangle a_{m,0}^* a_{m,1}, \quad (19)$$

with the direct and exchange matrix elements $\langle m0,k0 | V_{dx} | k0,m0 \rangle = 2\langle m0,k0 | V | k0,m0 \rangle - \langle m0,k0 | V | m0,k0 \rangle$. An example of the self-consistently calculated HF quasiparticle energies $E_{HF}(l)$ for $N_e=12$, $B=3$ T, and $\omega_0=6$ meV is shown in Fig. 6(a). Circles denote quasiparticle energies calculated without Landau-level mixing while bars show renormalized HF quasiparticle energies. The overall behavior of quasiparticles is similar. The self-consistent HF energies are, however, lower than the non-self-consistent ones.

A similar HF procedure can be applied to the center- and edge-spin-flip configurations, with the center configuration involving mixing of $|m=0,n=1\rangle$ and $|m=1,n=2\rangle$ (third-
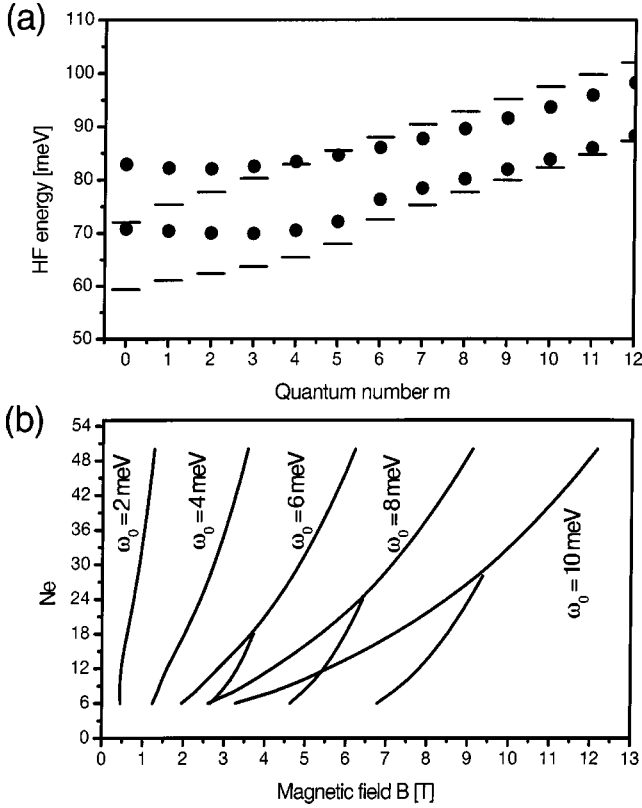
FIG. 6. (a) Hartree-Fock quasiparticle energies for a dot with eight electrons, confinement energy $\omega_0=6$ meV and in the magnetic field 3 T; the circles (bars) show the energies derived without (with) Landau-level mixing. (b) Phase diagram of the even-electron droplet as a function of the electron number and magnetic field in the Hartree-Fock approximation.

Landau-level) states. The resulting total energies can be compared to establish stability ranges of different phases. The resulting HF phase diagram for parameters identical to those in Fig. 4 is shown in Fig. 6. We see that the overall behavior of the phase diagram is similar without and with Landau-level mixing: there is a stable $\nu=2$ phase up to a critical number of electrons, N_c, which depends on confinement energy. However, the value of N_c and the values of critical fields are significantly different from those obtained in the LLL approximation.

B. Influence of correlations: Electron-hole pair excitations, LSDA, and exact diagonalization

The center- and edge-spin-flip processes described above involve singlet-triplet transitions; hence they are driven by exchange interaction. The HF approximation includes the exchange, but neglects electronic correlations. Correlations are known to counteract exchange, leading even to a collapse of the Zeeman gap for QHDs in the $\nu<2$ regime.[4] Therefore we attempt to include correlations into our model using three different approaches: (a) single electron-hole pair excitations from the self-consistent HF $\nu=2$ ground state, (b) the spin density functional theory (SDFT) LSDA calculation over a broad range of electron numbers, and (c) exact diagonalization for $N_e=6$ and $N_e=8$.

We start with one electron-hole pair excitation spectrum in the HF basis. Our HF procedure is spin and space restricted, so the angular momentum and the total spin S_z are good quantum numbers. We note that the eigenvector corresponding to the lowest HF eigenvalue of the self-consistent HF Hamiltonian determines coefficients $a^*_{m,0,\sigma}, a^*_{m,1,\sigma}$ not only for occupied but also for unoccupied angular momentum channels. These coefficients allow us to replace the two operators $c^\dagger_{m,0,\sigma}, c^\dagger_{m+1,1,\sigma}$ by a single operator $A^\dagger_{m,0,\sigma} = a^*_{m,0,\sigma}c^\dagger_{m,0,\sigma} + a^*_{m,1,\sigma}c^\dagger_{m+1,1,\sigma}$ for all channels. The second self-consistent operator $A^\dagger_{m,1,\sigma}$ can be naturally constructed from the eigenvector corresponding to the second excited HF orbital. We can therefore express our old creation operators $c^\dagger$ in terms of new operators $A^\dagger$ as $A^\dagger_{i,l} = \Sigma_j U_{i,j}(l)c^\dagger_{l+j,j}$ $(i,j=0,1)$ in each angular momentum and spin channel $l\sigma$ and obtain the Hamiltonian in the new basis:

$$H = \sum_{l,k,k',\sigma} t_{k,k'}(l)A^\dagger_{kl,\sigma}A_{k',l,\sigma}$$

$$+ \frac{1}{2}\sum_{k_1 l_1 k_2 l_2 k_3 l_3 k_4 l_4 \sigma\sigma'} \langle k_1 l_1 k_2 l_2|V|k_3 l_3 k_4 l_4\rangle$$

$$\times A^\dagger_{k_1 l_1 \sigma}A^\dagger_{k_2 l_2 \sigma'}A_{k_3 l_3 \sigma'}A_{k_4 l_4 \sigma}, \qquad (20)$$

where U is the transformation inverse to that obtained from HF minimization, and subsequent orthogonalization procedure.

The renormalized Coulomb matrix elements are expressed now in terms of angular momentum l and level index k in each angular momentum channel as

$$\langle k_1 l_1 k_2 l_2|V|k_3 l_3 k_4 l_4\rangle = \sum_{j_1 j_2 j_3 j_4} \langle j_1+l_1 k_1, j_2+l_2 k_2|V|j_3$$

$$+ l_3 k_3, j_4+l_4 k_4\rangle$$

$$\times U_{k_1,j_1}(l_1)U_{k_2,j_2}(l_2)$$

$$\times U_{k_3,j_3}(l_3)U_{k_4,j_4}(l_4). \qquad (21)$$

We see that the angular momentum structure of the two scattering particles is unchanged, but the distribution over Landau levels is changed. Similar considerations hold for the renormalized kinetic energy matrix:

$$t_{k,k'}(l) = \sum_j U_{kj}(l)U_{k'j}(l)\varepsilon_j(l), \qquad (22)$$

which is not diagonal in the HF basis.

For each angular momentum channel $L_{\nu=2} + \delta l$ we create electron-hole pair triplet excitations from the $\nu=2$ ground state, $A^\dagger_{k,l+\delta l\uparrow}A_{0l\downarrow}|\nu=2\rangle_{HF}$, where $k=0$ corresponds to an excitation to the first Landau level, possible only for $\delta l > 0$, and $k=1$ corresponds to an excitation to the second Landau level, possible for any $\delta l > -N$ for a $2N$-electron system. The correlated ground state wave function in this angular momentum channel can be then written, in terms of pair excitations, as $|\Psi(\delta l)\rangle = \Sigma_{k,l}D_{k,l}A^\dagger_{k,l+\delta l\uparrow}A_{0l\downarrow}|\nu$
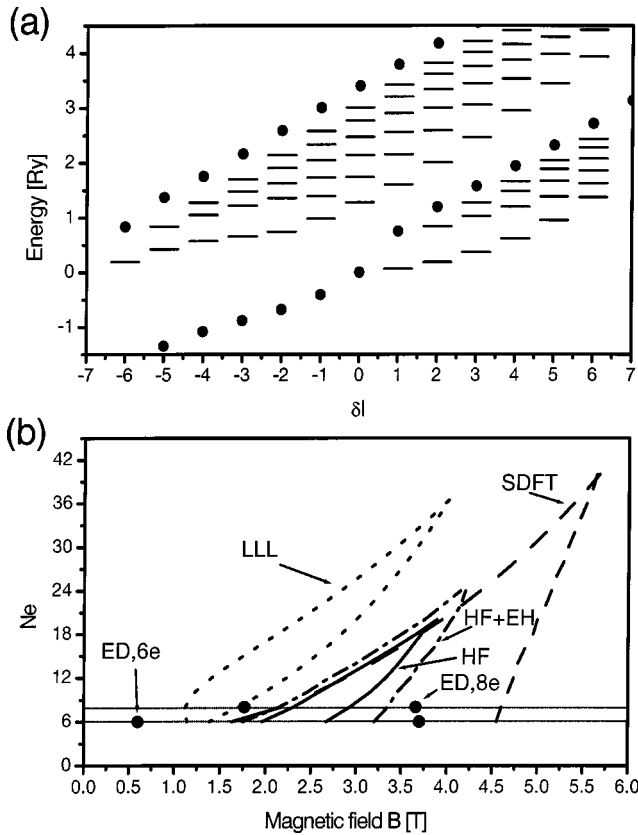
FIG. 7. (a) Pair excitation spectrum from the $\nu=2$ droplet for 12 electrons, $B=3$ T, $\omega_0=6$ meV for different angular momentum channels. Solid circles denote the Hartree-Fock quasiparticle energies, bars denote correlated triplet ground and excited states. (b) Phase diagrams obtained without Landau-level mixing (dotted lines), using Hartree-Fock approximation (solid lines), from single electron-hole pair excitation spectra (dot-dashed lines), using the SDFT-LSDA approach (dashed lines) and exact diagonalization (full circles).

$=2\rangle_{HF}$. The coefficients $D_{k,l}$ and energies of pair excitations are obtained by diagonalizing the Hamiltonian matrix (20).

The pair excitation spectrum calculated for $2N=12$, $B=3$ T, $\omega_0=6$ meV is shown in Fig. 7(a), together with HF quasiparticle energies. The energy scale was shifted in such a way that the energy of the $\nu=2$ ground state is zero (Zeeman energy is neglected). In the angular momentum channel $\delta l=-6$ there is only one state, because only one pair excitation is possible (this is the center-spin-flip configuration). With the increase of δl the number of inter–Landau level configurations increases. The lowest excitation in each angular momentum channel separates from a band and forms a collective inter-Landau-level spin-flip mode. Finally, at $\delta l=+1$ (the subspace of the edge spin flip), excitations to the first Landau level become possible, and from now on two broad bands of states, separated by a gap, are visible. The lowest energy excitation in each angular momentum channel $\delta l \geq 0$ also separates from a band and forms a collective intra-Landau-level edge-spin-flip mode. In this approach, the center-spin-flip state is not renormalized by correlations, but the edge spin flip configuration becomes correlated with

single electron-hole pair excitations to the second Landau level.

When the energy of spin-flip excitations for any angular momentum becomes lower than the HF ground state, a transition in the droplet takes place. We calculate these excitations over a broad range of electron numbers, magnetic field, and confining energies, and obtain the phase diagram. It is shown in Fig. 7(b) (dash-dotted lines). For comparison we also show the HF phase diagram obtained earlier without (dotted lines) and with Landau level mixing (solid lines). As can be seen, both self-consistent HF and single-pair excitation approximations predict (a) the phase boundaries to occur for magnetic fields higher by ~ 1 T, (b) the collapse of the $\nu=2$ phase to occur for smaller critical number of electrons N_c when compared to those obtained without Landau-level mixing.

Let us now compare the HF (solid lines) and the pair excitation (dash-dotted lines) approaches. In both of them the low-field $\nu=2$ phase boundary (center spin flip) is established by considering only one configuration. Therefore the small discrepancy between the results cannot be attributed to correlation effects, but rather to the difference between the two approaches. In the HF method the energy of each configuration is found by separate self-consistent procedures, in pair excitations only the $\nu=2$ configuration is considered self-consistently, and the center spin flip is an excitation from $\nu=2$. This effect also plays a role in the high-field $\nu=2$ phase boundary, but here the edge-spin-flip state is correlated with the configurations involving occupation of the second Landau level. Thus the influence of correlations counteracts the exchange, thereby broadening the $\nu=2$ phase stability range.

An alternative approach to include correlations for arbitrary electron number is to include exchange and correlation in the SDFT-LSDA approach. Its application proved insightful in the study of many ground state properties of artificial atoms and molecules.[5,20,29–36] We apply the local spin density approximation using the Tanatar-Ceperley parametrization of the exchange-correlation potential as a function of the density parameter r_s and polarization ξ.[37] As we do not aim at current effects in particular we refrained from using a current spin-density functional theory approach using the parametrization of the exchange correlation energy as a function of density parameter, polarization, and filling factor.[38–40] Furthermore, the reported differences for GS energies between the SDFT and CSDFT methods are negligible,[33] and for low electron numbers comparisons of the magnetic fields where the GS transitions take place show a good agreement between the SDFT and exact diagonalization methods[41] even in medium magnetic fields. To remain consistent with previous approximations, we took only two Landau levels as the variational space for the calculation. Considering its quantum numbers L and S_z the GS energy of each configuration was calculated. The result is shown in Fig. 7(b) (dashed lines). The low-field $\nu=2$ stability edge calculated here does not differ substantially from that obtained previously. However, due to correlations, the $\nu=2$ stability range is now increased by 1.5 T. Moreover, the spin singlet remains stable up to $N_c=38$ electrons, a number twice that predicted by HF

approximation. This stability is also due to the influence of correlations: the exchange effects lower only the energy of spin-polarized states, while correlation effects provide a mechanism to decrease ground state energies for the spin-singlet configuration as well.

On the basis of the comparison of several approaches we see that the stability of the spin-singlet droplet is a sensitive function of correlations. Different approximations give qualitatively similar results but differ significantly in quantitative predictions.

In order to gauge the validity of different approximations, we calculated the phase diagram using exact diagonalization techniques for electron numbers $N_e = 6$ and $N_e = 8$. Details of this approach will be published elsewhere.[41] Here we only note that in this calculation the total angular momentum, total spin, and total S_z were resolved as good quantum numbers. It reduced the Hilbert space for each set of quantum numbers to a computable size, so that within the two-Landau-level approximation both exchange and correlations are treated exactly. The results are shown in Fig. 7(b) (full circles). For $2N = 6$ we see a stability region of the $\nu = 2$ phase much broader than that from the pair excitation approximation, but the discrepancy becomes much smaller for a larger number of electrons, where the self-consistent approach is expected to work better. However, the discrepancy between the exact diagonalization and the SDFT-LSDA results does not seem to improve with the increase of the electron number. To analyze this problem we calculated phase diagrams for $2N = 6$ electrons using SDFT-LSDA and exact diagonalization including three Landau levels. The results (not shown here) indicate that the spin density profiles do not change dramatically with the increase of the number of Landau levels, and therefore the SDFT phase diagram remains similar to that in Fig. 7 (b). On the other hand, the Hilbert space size in the exact diagonalization increases by orders of magnitude, which affects the phase diagram, shifting it towards higher magnetic fields. Approximate calculations for eight Landau levels reveal a good agreement between SDFT and exact diagonalization, and we rely on predictions of SDFT for large electron numbers in what follows.

V. CB AMPLITUDE REVERSAL

Up to now we discussed the $\nu = 2$ line as the set of features in the position of CB lines reflecting the transfer of one electron from the center to the edge of the QHD. We assumed the electron number to be small enough, so that this transition involved the spin-singlet configuration of the even-electron QHD. We established that the existence of pairs of cusps seen in the CB trace was due to a different energy dependence of the center and edge orbitals on the magnetic field. We now turn to describing the behavior of the droplet in the vicinity of the critical electron number N_c, where the spin-singlet configuration ceases to be the ground state. As can be seen in Figs. 6 and 7(b), beyond N_c the $\nu = 2$ line is continued by another phase boundary, separating the center-spin-polarized and the edge-spin-polarized configurations. The transition between these two phases involves the transfer of one electron from the center to the edge of the QHD, but

this time the final state is a spin triplet. Because of that the continuation of the $\nu = 2$ line in the CB trace will exhibit a pair of cusps similar to that observed for a the electron number $2N < N_c$. Thus the CB peak *position* spectroscopy is not expected to reveal any indication of the collapse of the spin-singlet phase.

The tunneling spectroscopy conducted in the regime of spin-polarized injection or detection[28] allows, however, to extract information also from the CB peak *amplitude*. In this regime the energy separation of two different spin species in the two-dimensional electron gas (2DEG) making up the source and drain reservoirs is converted to the spatial separation of electrons with different spin orientations at the edge of the 2DEG.[4,28] This spatial separation at the edge drastically influences the tunneling probability of electrons with different spin to and from a quantum dot. Now the electrons injected into the dot are predominantly spin down. Moreover, the tunneling matrix elements are dominated by the overlap of the wave functions of the dot and the reservoirs. Therefore the tunneling event is allowed if the extra spin-down electron is added to (or removed from) the edge of the QHD. If the extra electron is spin up, the current amplitude is expected to be much smaller (spin blockade), and if we add a spin-down electron to the center, the current amplitude is small due to small wave function overlap. This spin-resolved tunneling should then be sensitive to the collapse of the spin-singlet phase; therefore we now focus on the understanding of CB amplitude patterns both below and above the critical electron number.

A. Configurations and corresponding amplitudes

Let us first consider the system of noninteracting electrons with artificially enhanced Zeeman energy (Fig. 1). The collapse of the $\nu = 2$ phase takes place when the energy of the center orbital crosses the first edge-spin-flip line denoted by full circles, i.e., at the magnetic field 7.8 T, for $N_c = 14$ electrons.

The configurations adjacent to the $\nu = 2$ line in the regime of small number of electrons ($2N < N_c$) are schematically shown in Fig. 8(a) for four neighboring electron numbers, $2N$ through $2N + 3$. Let us analyze systematically the expected amplitude pattern starting with the addition of one electron to the $2N$-electron QHD. For low magnetic field we add the electron to the center configuration with $2N$ electrons to obtain the center configuration as a final state of the $(2N + 1)$-electron system. The extra electron is added at the edge in a spin-down orbital. As the injected electrons are mainly spin-down the spin blockade causes the tunneling current amplitude to be small. As we increase the magnetic field, the $2N$-electron QHD undergoes a transition to the spin singlet. The extra electron must be added to the center, but due to small overlap of wave functions the tunneling amplitude is very small. Finally, the $(2N + 1)$-electron QHD undergoes a center-edge transition. In this range of magnetic field the extra electron spin down is added to the edge, so we expect the tunneling current to have a high amplitude.

Let us now add one electron to the $(2N + 1)$-electron system. For low magnetic fields both $(2N + 1)$- and $(2N + 2)$-electron systems are in the respective center con-
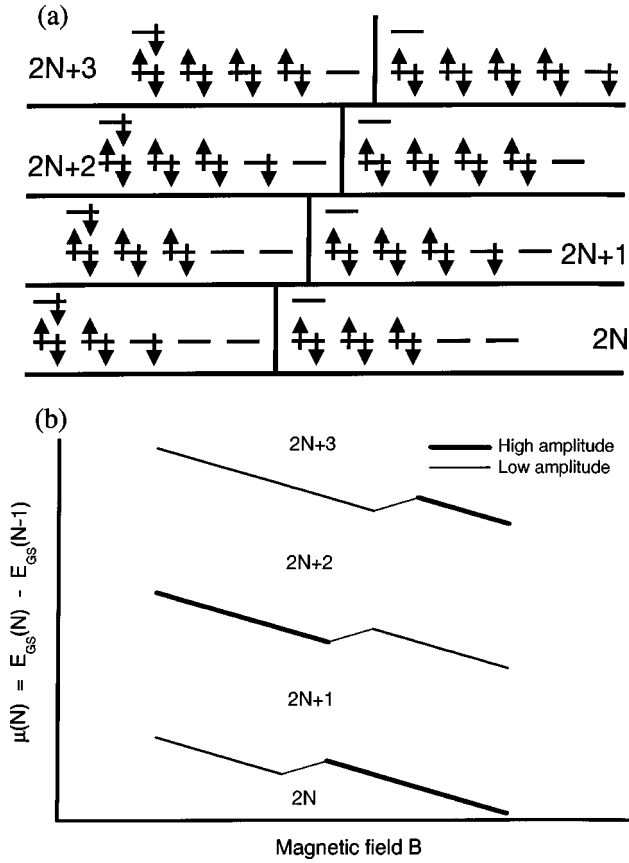
FIG. 8. (a) Ground state configurations and (b) schematic addition and amplitude spectrum in the vicinity of the $\nu=2$ line for QHD with small number of electrons.
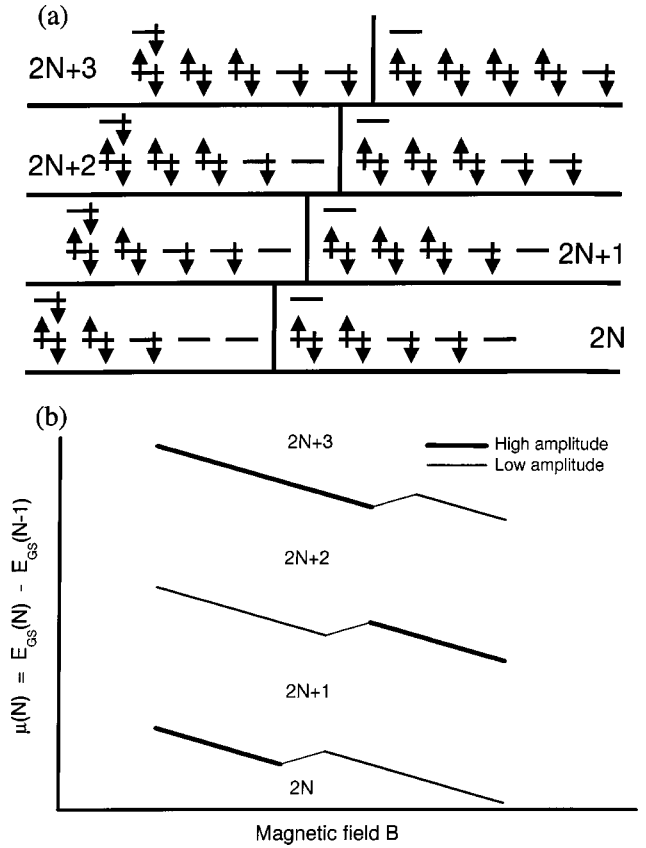

FIG. 9. (a) Ground state configurations and (b) schematic addition and amplitude spectrum in the vicinity of the $\nu=2$ line for QHD with large number of electrons.

figurations. They differ by one spin down electron at the edge, so the tunneling current amplitude is high. For intermediate magnetic fields the $(2N+1)$-electron droplet exhibits the electron transfer to the edge and we must add the spin-down electron to the center, which causes the amplitude to be small. For higher magnetic fields the $(2N+2)$-electron droplet becomes a spin singlet, the extra electron must be added at the edge, but with spin up. The spin blockade causes the amplitude to be low. The traces of CB peaks corresponding to these transitions are shown in Fig. 8(b), with thicker lines marking the sections where a high amplitude is expected.

If the number of electrons $2N>N_c$, the spin-singlet phase is no longer stable, and the configurations adjacent to the $\nu=2$ line are slightly different than those in the normal regime (see Fig. 9). The center configuration for odd-electron numbers, instead of being a singlet with one extra electron in the center, acquires a spin-polarized edge. Similarly, the edge configuration for even-electron numbers, previously a spin singlet, becomes edge-spin-polarized. These new configurations strongly influence the addition amplitudes. Upon careful consideration of spin blockade and overlap conditions, we find that now the amplitude pattern is opposite to that observed in the normal regime: the amplitude is high on the low-magnetic-field side of the $\nu=2$ line when we add an extra electron to the even-electron system. This is summarized in the addition spectrum shown in Fig. 9(b).

As we can see, the collapse of the $\nu=2$ phase manifests itself in the CB spectroscopy by the reversal of the CB current amplitude patterns, as observed in recent experiments.[28] However, when we increase the magnetic field and the number of electrons further, we encounter the second edge-spin-flip line, denoted in Fig. 1 by full circles. In this regime the configurations adjacent to the $\nu=2$ line will change, resulting in yet another modification of the amplitude pattern. This increasing complexity forces us to go beyond a qualitative model and examine the influence of interactions on our system.

B. Mean-field calculations

We choose two complementary approaches discussed previously: the HF approach in two-Landau-level approximation and the SDFT-LSDA approach. This choice permits us to examine the influence of direct and exchange interactions and of correlations separately.

The HF analysis is carried out in the way described before, but now it is extended to configurations of both odd and even electron numbers with a more highly polarized edge. We used the parameters $\omega_0=6$ meV and $E_z=0.02$ meV/T. The resulting phase diagrams are shown in Fig. 10. For even electron numbers we observe the breakdown of the $\nu=2$ phase at $2N=20$ electrons. However, the higher polarized phases do not align favorably for the system to exibit the
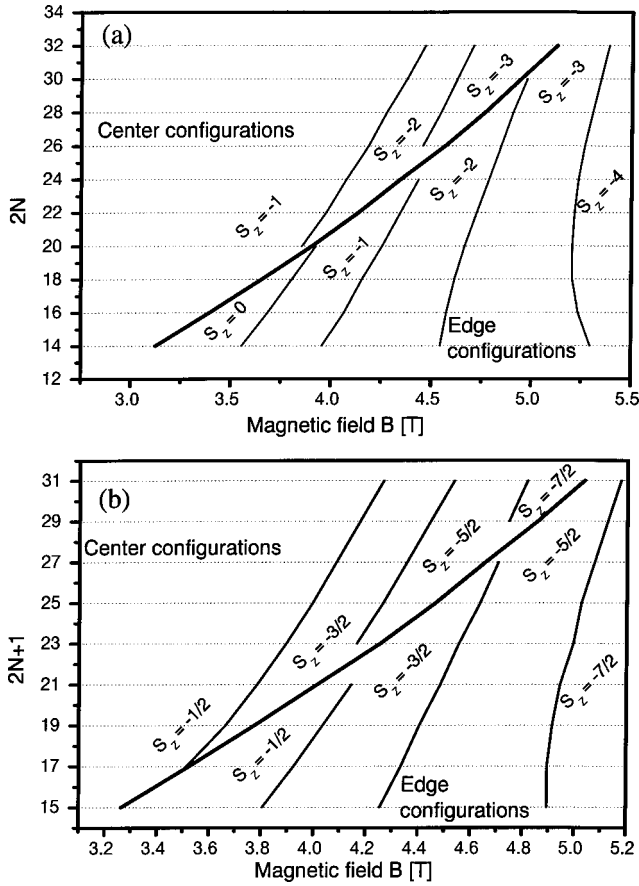
FIG. 10. Phase diagram of the interacting system with GaAs Zeeman energy for (a) even and (b) odd electron numbers in the HF approximation. The center and edge configurations are separated by the thick line, and the states for even and odd electron numbers can be identified by their spin quantum number.
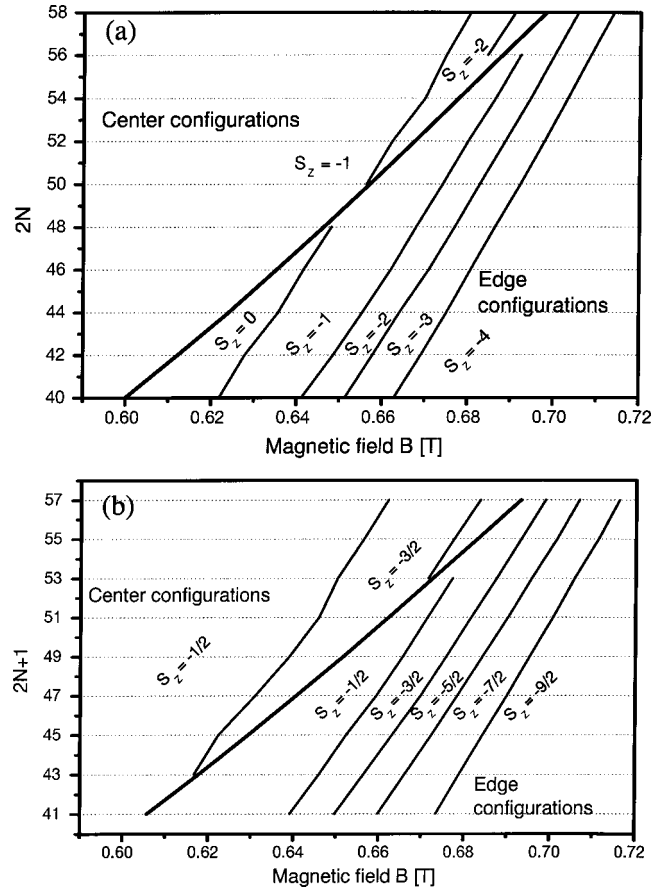

FIG. 11. Phase diagram of the interacting system with GaAs Zeeman energy for (a) even and (b) odd electron numbers in the SDFT-LSDA approximation including 10 Landau levels. The center and edge configurations are separated by the thick line, and the states for even- and odd-electron numbers can be identified by their spin quantum number.

reversal of amplitudes. In order to observe it, we need to have the center and edge configurations both with total $S_z = -1$ neighboring the $\nu = 2$ line. However, as can be seen from Fig. 10(a), the center configuration with $S_z = -1$ ceases to be stable in favor of the more highly spin-polarized center configuration with $S_z = -2$ right at the magnetic field and the electron number for which the spin singlet collapses. Compared to the single-particle picture this transition is shifted to much lower magnetic fields. Therefore it can be argued that the favorable alignment of phases takes place just for one electron number, $2N = 20$. As for the odd electron numbers [Fig. 10(b)], the phases are aligned favorably for $2N + 1 = 19$ and 21 electrons.

So, the characteristic reversal of amplitudes predicted in the single-particle picture will be now observed only in transitions from 19- to 20-electron and from 20- to 21-electron QHD. The reason for this behavior of the system is the overestimation of the exchange interaction by the HF approach. Because of that, the spin-polarized configuration with total $S_z = -2$ will have artificially lowered energy with respect to the configuration with total $S_z = -1$ and the transition between these two configurations will occur too early. We established earlier that correlations can counteract these artifi-

cially enhanced exchange interactions. Therefore we will now generate the analogous phase diagrams using the SDFT-LSDA approximation.

In what follows, in order to provide a sufficient variational space for the DFT algorithm, we took into account a single-particle basis set with quantum numbers $n = 0, \ldots, 9$ and $m = 0, \ldots, 59$, i.e., ten Landau levels. To make contact with experiment, the confinement energy $\omega_0 = 1$ meV, close to the value observed experimentally,[28] has been used. We carried out two calculations: for the normal GaAs Zeeman energy $E_Z = 0.02$ meV/T (Fig. 11) and for the Zeeman energy artificially enhanced by a factor of 2 (Fig. 12). Let us focus on the odd-electron numbers first. Compared to the HF calculation, the range of favorable alignment of phases has been vastly extended—to five electron numbers (43 through 51) for normal Zeeman energy, and even seven electron numbers (35 through 47) for enhanced Zeeman energy. For even electron numbers we observe the breakdown of the spin-singlet phase for $N_c = 48$ and 38 electrons with normal and doubled Zeeman energy, respectively. However, in Fig. 11 for normal Zeeman energy the favorable alignment of phases is again seen only for one electron number, $2N = 50$, so the amplitude reversal is predicted only for QHD
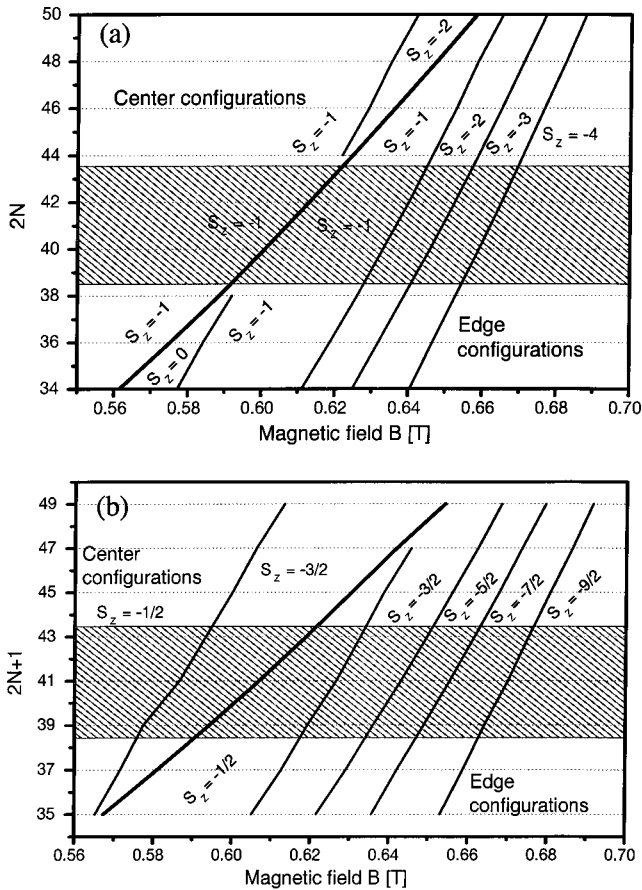
FIG. 12. Phase diagram of the interacting system with doubled Zeeman energy for (a) even and (b) odd electron numbers in the SDFT-LSDA approximation including 10 Landau levels. The center and edge configurations are separated by the thick line, the states for even and odd electron numbers can be identified by their spin quantum number. The shaded areas mark the regime that shows a reversal of amplitudes.

transitions from 49 to 50 electrons and from 50 to 51 electrons. The situation is improved only by enhancing the Zeeman energy (Fig. 12 (a)), which shifts down the energies of spin-polarized configurations without changing the energy of the spin singlet. As a result the collapse of the $\nu=2$ phase takes place for lower magnetic fields and lower electron number, and the spin flips in question are finally disaligned. We then find a stable reversal of the amplitude modulation for QHDs with 38 to 43 electrons. Note that the sole purpose of enhancing the Zeeman energy was to favor spin-polarized configurations over the spin singlet. This goal could be also attained by including more exchange interaction, perhaps slightly underestimated in the SDFT. Another reason for emphasizing exchange effects is the screening of the interaction by the metal gates of the device.[28] The screening decreases long-range correlations while it does not influence the short-range exchange effects. Therefore the reversal of amplitude patterns is very sensitive to the balance between exchange and correlations.

VI. CONCLUSIONS AND OUTLOOK

We investigated the physics of the $\nu=2$ quantum Hall droplet as a function of the electron number, confinement energy, and the magnetic field. We considered the spin-singlet configuration and compared its energy to the energies of configurations with increasing spin polarization, both for even and odd electron numbers. We found that there exists a critical number of electrons N_c, beyond which the spin-singlet phase ceases to be stable at any magnetic field. Then, by considering the energies of configurations adjacent to the $\nu=2$ line for the $2N$ system, and comparing them to those of the $2N+1$ system, we established the characteristic shape of the addition spectra, due to center-edge electronic transitions in the initial or final state. We studied the same configurations in different approaches (HF, electron-hole pair excitation spectra, and SDFT-LSDA) to take into account the electron-electron interactions. All our calculations clearly show the breakdown of the $\nu=2$ quantum Hall droplet as a GS configuration with increasing number of electrons and magnetic field. However, depending on the method, this breakdown occurs in different regimes. The Hartree-Fock calculations, treating the exchange energy but neglecting correlations, uncover the basic renormalization effects of the interaction. It acts effectively as an enhanced Zeeman energy, lowering the energies of spin-polarized states compared to the noninteracting picture, and causing the spin-flip transitions to occur for experimentally observed magnetic fields (below 10 T), and the collapse of the spin-singlet phase for a critical number of electrons of the order of $N_c \sim 30$. The inclusion of correlations, carried out by employing the electron-hole pair excitation approach, the SDFT-LSDA approximation, and exact diagonalization techniques leads to a broadening of the stability range of the spin singlet phase both in magnetic field and in electron number. The reason for this is that unlike the exchange, correlations lower the energies of spin singlet as well as spin-polarized configurations.

Then we turned to predicting the signature of the collapse of the spin-singlet phase in the addition spectrum. We found that it will not be revealed in the Coulomb blockade peak position, but will be manifested by a reversal of the CB current-amplitude patterns. This reversal of amplitudes is almost not recovered upon the inclusion of interactions if the approximation used overestimates exchange or correlations. However, if a proper balance between them is found (e.g., by using an enhanced Zeeman energy), the reversal of amplitude pattern is obtained for a range of electron numbers. These theoretical predictions regarding both CB peak position and amplitude spectra are observed experimentally.[28]

A theoretically and experimentally interesting problem not discussed here is the multiple reversal of the amplitude pattern as suggested by consideration of the noninteracting system. Unfortunately, the experimental investigations have not yet been carried out up to high enough electron number to observe it.

[1] For reviews and references see L. Jacak, P. Hawrylak, and A. Wójs, *Quantum Dots* (Springer, Berlin, 1998); L. P. Kouwenhoven, C. M. Marcus, P. McEuen, S. Tarucha, R. Westervelt and N. S. Wingreen, in *Mesoscopic Electron Transport*, edited by L. L. Sohn, L. P. Kouwenhoven and G. Schon, Series E (Kluwer, Amsterdam, 1997), p. 345; R. C. Ashoori, Nature (London) **379**, 413 (1996); M. Kastner, Phys. Today **46** (1), 24 (1993); T. Chakraborty, Comments Condens. Matter Phys. **16**, 35 (1992).

[2] M. Ciorga, A.S. Sachrajda, P. Hawrylak, C. Gould, P. Zawadzki, Y. Feng, and Z. Wasilewski, Phys. Rev. B **61**, R16 315 (2000).

[3] S. Tarucha, D.G. Austing, Y. Tokura, W.G. van der Wiel, and L.P. Kouvehoven, Phys. Rev. Lett. **84**, 2485 (2000).

[4] P. Hawrylak, C. Gould, A.S. Sachrajda, Y. Feng, and Z. Wasilewski, Phys. Rev. B **59**, 2801 (1999).

[5] D.G. Austing, S. Sasaki, S. Tarucha, S.M. Reimann, M. Koskinen, and M. Manninen, Phys. Rev. B **60**, 11 514 (1999).

[6] S. Tarucha, D.G. Austing, T. Honda, R.J. van der Haage, and L. P. Kouwenhoven, Phys. Rev. Lett. **77**, 3613 (1996).

[7] R.C. Ashoori, H.L. Stormer, J.S. Weiner, L.N. Pfeiffer, K.W. Baldwin, and K.W. West, Phys. Rev. Lett. **71**, 613 (1993).

[8] P.L. McEuen, E.B. Foxman, U. Meirav, M.A. Kastner, Y. Meir, N.S. Wingreen, and S.J. Wind, Phys. Rev. Lett. **66**, 1926 (1991); P.L. McEuen, E.B. Foxman, J.M. Kinaret, U. Meirav, M.A. Kastner, N.S. Wingreen, and S.J. Wind, Phys. Rev. B **45**, 11 419 (1992).

[9] O. Klein, S. de Chamon, D. Tang, D. M. Abusch-Magder, U. Meirav, X.-G. Wen, M. A. Kastner, and S. J. Wind, Phys. Rev. Lett. **74**, 785 (1995).

[10] T. H. Oosterkamp, J. W. Janssen, L. P. Kouwenhoven, D. G. Austing, T. Honda, and S. Tarucha, Phys. Rev. Lett. **82**, 2931 (1999).

[11] A.S. Sachrajda, R.P. Taylor, C. Dharma-wardana, P. Zawadzki, J.A. Adams, and P. T. Coleridge, Phys. Rev. B **47**, 6811 (1993).

[12] D.R. Stewart, D. Sprinzak, C.M. Marcus, C.I. Duruoz, and J.S. Harris, Science **278**, 1784 (1997).

[13] J. Weis, R.J. Haug, K. von Klitzing, and K. Ploog, Phys. Rev. Lett. **71**, 4019 (1993).

[14] R.H. Blick, D. Pfannkuche, R.J. Haug, K. von Klitzing, and K. Eberl, Phys. Rev. Lett. **80**, 4032 (1998).

[15] P. Hawrylak, Phys. Rev. Lett. **71**, 3347 (1993).

[16] A. H. MacDonald, S. R. Eric Yang, and M. D. Johnson, Aust. J. Phys. **46**, 345 (1993).

[17] S.R. Eric Yang, A.H. MacDonald, and M.D. Johnson, Phys. Rev. Lett. **71**, 3194 (1993).

[18] X. G. Wen, Phys. Rev. B **41**, 12 838 (1990); C. de Chamon and X.-G. Wen, *ibid.* **49**, 8227 (1994).

[19] H.-M. Müller, and S.E. Koonin, Phys. Rev. B **54**, 14 532 (1996).

[20] S.M. Reimann, M. Koskinen, M. Manninen, and B.R. Mottelson, Phys. Rev. Lett. **83**, 3270 (1999).

[21] J.H. Oaknin, L. Martin-Moreno, and C. Tejedor, Phys. Rev. B **54**, 16 850 (1996); J.J. Palacios, L. Martin-Moreno, G. Chiappe, E. Louis, and C. Tejedor, *ibid.* **50**, 5760 (1994).

[22] H. Imamura, H. Aoki, and P.A. Maksym, Phys. Rev. B **57**, R4257 (1998).

[23] P. Hawrylak, Phys. Rev. B **51**, 17 708 (1995).

[24] A. Wojs and P. Hawrylak, Phys. Rev. B **56**, 13 227 (1997).

[25] M. Ciorga, A. Wensauer, M. Pioro-Ladriere, M. Korkusinski, J. Kyriakidis, A.S. Sachrajda, and P. Hawrylak, Phys. Rev. Lett. **88**, 256804 (2002).

[26] A. Wojs and P. Hawrylak, Phys. Rev. B **53**, 10 841 (1996).

[27] P. Hawrylak, Solid State Commun. **88**, 475 (1993).

[28] M. Ciorga, A.S. Sachrajda, P. Hawrylak, C. Gould, P. Zawadzki, Y. Feng, and Z. Wasilewski, Physica E (Amsterdam) **11**, 35 (2001); A.S. Sachrajda, P. Hawrylak, M. Ciorga, C. Gould, and P. Zawadzki, *ibid.* **10**, 493 (2001).

[29] M. Ferconi and G. Vignale, Phys. Rev. B **56**, 12 108 (1997).

[30] M. Koskinen, M. Manninen, and S.M. Reimann, Phys. Rev. Lett. **79**, 1389 (1997).

[31] K. Hirose and N.S. Wingreen, Phys. Rev. B **59**, 4604 (1999).

[32] A. Puente and Ll Serra, Phys. Rev. Lett. **83**, 3266 (1999).

[33] O. Steffens, U. Rössler, and M. Suhrke, Europhys. Lett. **42**, 529 (1998).

[34] O. Steffens and M. Suhrke, Phys. Rev. Lett. **82**, 3891 (1999).

[35] A. Wensauer, O. Steffens, M. Suhrke, and U. Rössler, Phys. Rev. B **62**, 2605 (2000).

[36] A. Wensauer, J. Kainz, M. Suhrke, and U. Rössler, Phys. Status Solidi B **224**, 675 (2001).

[37] B. Tanatar and D.M. Ceperley, Phys. Rev. B **39**, 5005 (1989).

[38] M. Rasolt and F. Perrot, Phys. Rev. Lett. **69**, 2563 (1992).

[39] G. Fano and F. Ortolani, Phys. Rev. B **37**, 8179 (1988).

[40] D. Levesque, J.J. Weis, and A.H. MacDonald, Phys. Rev. B **30**, 1056 (1984).

[41] A. Wensauer, M. Korkusinski, and P. Hawrylak (unpublished).